AIP | Applied Physics Letters

AlInAsSb separate absorption, charge, and multiplication avalanche photodiodes

Min Ren, Scott J. Maddox, Madison E. Woodson, Yaojia Chen, Seth R. Bank, and Joe C. Campbell

Citation: Applied Physics Letters **108**, 191108 (2016); doi: 10.1063/1.4949335
View online: http://dx.doi.org/10.1063/1.4949335
View Table of Contents: http://scitation.aip.org/content/aip/journal/apl/108/19?ver=pdfcov
Published by the AIP Publishing

AlInAsSb separate absorption, charge, and multiplication avalanche photodiodes

Min Ren,[1] Scott J. Maddox,[2] Madison E. Woodson,[1] Yaojia Chen,[1] Seth R. Bank,[2] and Joe C. Campbell[1,a)]
[1]Department of Electrical and Computer Engineering, University of Virginia, Charlottesville, Virginia 22904, USA
[2]Microelectronics Research Center, University of Texas, Austin, Texas 78758, USA

(Received 8 April 2016; accepted 27 April 2016; published online 11 May 2016)

We report $Al_xIn_{1-x}As_ySb_{1-y}$ separate absorption, charge, and multiplication avalanche photodiodes (APDs) that operate in the short-wavelength infrared spectrum. They exhibit excess noise factor less or equal to that of Si and the low dark currents typical of III-V compound APDs. *Published by AIP Publishing.* [http://dx.doi.org/10.1063/1.4949335]

Until the early 2000s avalanche photodiodes (APDs) were widely deployed in 10 Gb/s high performance optical receivers.[1,2] In subsequent years, the use of APDs for high-capacity systems declined as a result of their limited gain-bandwidth, the transition to coherent detection, and the development of high efficiency modulation techniques. Recently, the rapid growth of optical-fiber communications systems that utilize baud rates up to 25 Gbit/s as represented by 100-Gbit/s Ethernet (100 GbE) has led to a resurgence of research on APDs.[3] Two figures of merit for APD optical receivers are the excess noise factor and the gain-bandwidth product. Both are linked to the k factor, which is the ratio of the electron, α, and hole, β, ionization coefficients. The mean-squared shot-noise current can be expressed as[4]

$$\langle i_{shot}^2 \rangle = 2q(I_{ph} + I_{dark})M^2F(M)\Delta f, \quad (1)$$

where I_{ph} and I_{dark} are the primary photocurrent and dark current, respectively, M is the avalanche gain, Δf is the bandwidth, and $F(M)$ is the excess noise factor. In the local field model[4] the excess noise factor is given by

$$F(M) = kM + (1-k)(2-1/M). \quad (2)$$

The excess noise factor increases with increasing gain but increases more slowly for lower values of k. It follows that higher receiver sensitivities are achieved with low k values. The gain-bandwidth product is important because it is essential that the APD operates at sufficiently high gain to overcome the noise limitation of the following amplifier at the transmission bit rate. Emmons has shown that the lower the k value, the higher the gain bandwidth product of an APD.[5] Initially, for bit rates $\leq$10 Gb/s, InP/InGaAs APDs were the photodetectors that achieved the highest receiver sensitivities.[6–8] However, the relatively high k value of InP, $k \sim 0.5$, resulted in high excess noise and gain-bandwidth products of $<$100 GHz. Recently, Nada *et al.* have reported AlInAs/InGaAs APDs, for which the k value is $\sim$0.2; these APDs achieved 235 GHz gain-bandwidth product and receiver sensitivity of -21 dBm at 25 Gb/s and 10^{-12} bit error rate.[9] However, the "champion" material candidate for high performance APDs is Si. It has demonstrated k values $\sim$0.02 and gain-bandwidth products $>$340 GHz.[10] Unfortunately, as is well known, the bandgap of Si obviates operation at wavelengths $>1.0\,\mu$m. There have been many efforts in the past 20 years to achieve the low noise and high gain-bandwidth product of Si at telecommunications wavelengths (1.3 μm to 1.6 μm). One approach to utilize the excellent gain characteristics of Si has been to combine a Ge absorption region with a Si multiplication layer in a separate absorption, charge, and multiplication (SACM) APD.[10–13] In optical receivers, these APDs have achieved sensitivities as high as those of the best III-V compound APDs but not superior, as would have been expected from their low k value. This sensitivity limitation stems from the high dark current that arises from the lattice mismatch between Ge and Si, which contributes enough to the noise to offset the lower excess noise factor.

In this paper, we report separate absorption, charge, and multiplication (SACM) APDs fabricated from $Al_xIn_{1-x}As_ySb_{1-y}$, grown on GaSb. The excess noise factor of the $Al_{0.7}In_{0.3}As_{0.3}Sb_{0.7}$ multiplication region is characterized by a k value of $\sim$0.01, which is comparable with, or below, that of Si. Further, the lattice-matched $Al_{0.4}In_{0.6}As_{0.6}Sb_{0.4}$ absorbing region extends the operating wavelength to the short-wavelength infrared (SWIR) spectrum and offers gains as high as 50. These APDs achieve noise comparable with state-of-the-art Si APDs while maintaining low dark current similar to that of short-wavelength infrared (SWIR) III-V compound APDs and significantly less than Ge on Si APDs.

The epitaxial layers were grown on n-type Te-doped GaSb (001) substrates by solid-source molecular beam epitaxy (MBE). In order to bypass the wide miscibility gap present in the $Al_xIn_{1-x}As_ySb_{1-y}$ material system, these layers were grown as a digital alloy of the binary alloys AlAs, AlSb, InAs, and InSb, using a digital alloy period of 3 nm and the following layer sequence: AlSb, AlAs, AlSb, InSb, InAs, and Sb.[14,15] This approach has enabled a number of devices, including the first working staircase APD and low-noise $Al_{0.7}In_{0.3}As_{0.3}Sb_{0.7}$ APD.[16,17] Photoluminescence results indicate that the bandgap of $Al_{0.4}In_{0.6}As_{0.6}Sb_{0.6}$ is $\sim$0.7 eV, and the bandgap of $Al_{0.7}In_{0.3}As_{0.3}Sb_{0.7}$ is 1.16 eV.[15] By combining and utilizing their advantages, infrared photons can be absorbed in $Al_{0.4}In_{0.6}As_{0.6}Sb_{0.6}$ layer and photo-generated carriers can be multiplied in $Al_{0.7}In_{0.3}As_{0.3}Sb_{0.7}$. A schematic cross section of

a)jcc7s@virginia.edu

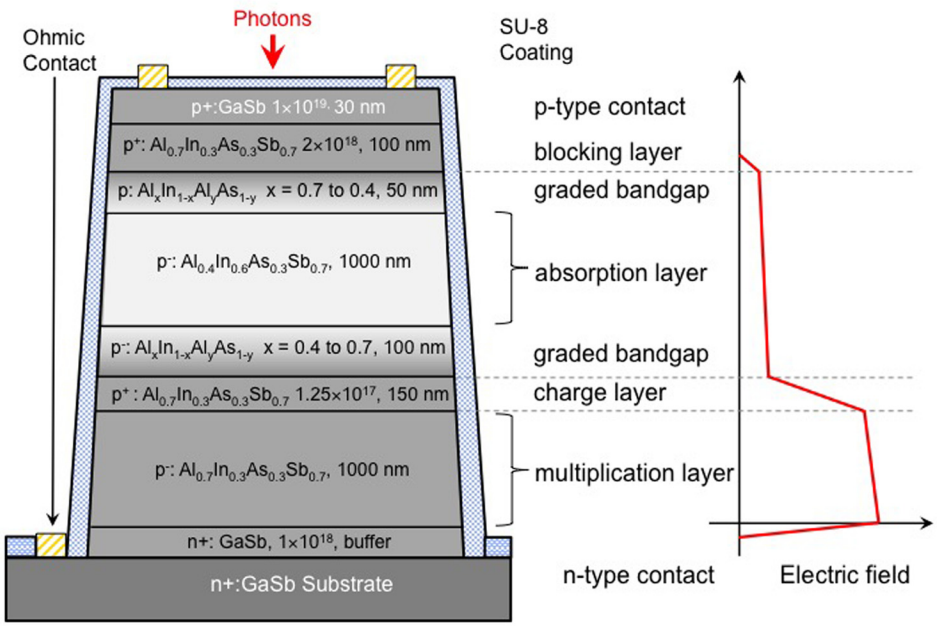

FIG. 1. Schematic cross section and electric field profile of $Al_xIn_{1-x}As_ySb_{1-y}$ SACM APD.

the $Al_xIn_{1-x}As_ySb_{1-y}$ SACM APD is shown in Figure 1. The structure includes a top GaSb contact layer. Beneath the p-type contact layer is a p^+: $Al_{0.7}In_{0.3}As_{0.3}Sb_{0.7}$ ($2\times10^{18}\,cm^{-3}$, 100 nm) blocking layer. The p^-: $Al_{0.4}In_{0.6}As_{0.6}Sb_{0.4}$ (1000 nm) absorbing layer is sandwiched between two 100 nm-thick p^+: $Al_xIn_{1-x}As_ySb_{1-y}$ regions in which the Al composition is graded between x = 0.4 and 0.7. Beneath the absorbing region is a p^+:$Al_{0.7}In_{0.3}As_{0.3}Sb_{0.7}$ ($1.25\times10^{17}\,cm^{-3}$, 150 nm) charge layer, the p^-: $Al_{0.7}In_{0.3}As_{0.3}Sb_{0.7}$ (1000 nm) multiplication layer, and an n^+: GaSb, $1–9\times10^{17}$ n-type contact layer. When reverse biased, strong electric field is formed in the multiplication layer to enable impact ionization, while low electric field is limited by charge layer in absorption layer to help photoelectron drifting. When reverse biased at 50 V, simulation indicates that the average electric field strengths in the absorption and the multiplication layers are <100 kV/cm and ~800 kV/cm, respectively.

Circular mesas were defined by using standard photolithography and N_2/Cl_2 inductive coupled plasma (ICP) dry etching. Etching was terminated with a surface-smoothing treatment of bromine methanol. In order to improve passivation and thus reduce the surface leakage current, an SU-8 coating was spun on immediately after the surface treatment. Titanium/gold contacts were deposited by e-beam evaporation onto the mesa and the substrate.

The dark current, photocurrent, and gain versus bias voltage of a 50 μm-diameter SACM APD are shown in Figure 2(a). The dark current at 95% breakdown is $\sim$120 nA, which is approximately 100× lower than that of Ge on Si APDs and comparable with that of AlInAs/InGaAs APDs.[9–13,18] The gain is plotted on the right vertical axis. Gain values as high as 50 have been observed. A Monte Carlo simulation was employed to study the multiplication mechanism. The Monte Carlo model in this paper is based on that in Ref. 19. The impact ionization rate, P_{ii}, is calculated using the Keldysh formula[20]

$$P_{ii} = \begin{cases} 0, & if\ E < E_{th} \\ C_{ii}\left(\dfrac{E}{E_{th}} - 1\right)^r, & if\ E \geq E_{th}. \end{cases} \quad (3)$$

The phonon scattering rate, C_{ii}, and threshold energy, E_{th}, are treated as fitting parameters. Some important model parameters are listed in Table I. A good fit to the measured

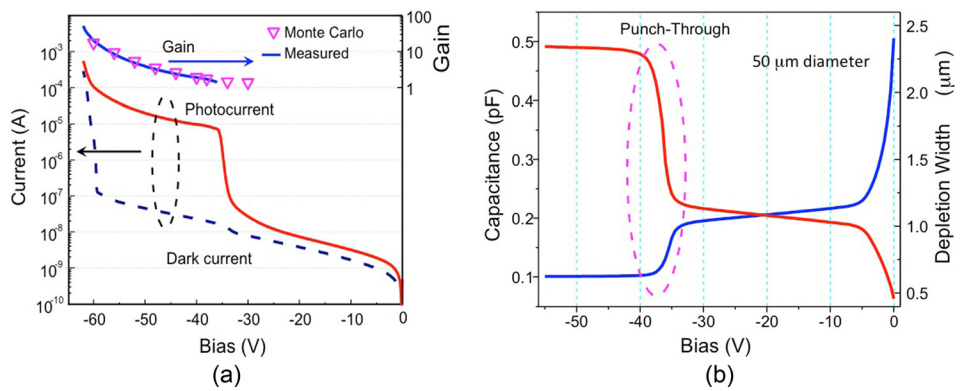

FIG. 2. (a) Dark current, photocurrent, measurement and simulation data (▽) of gain versus reverse bias of a 50-μm-diameter $Al_xIn_{1-x}As_ySb_{1-y}$ SACM APD at 300 K. (b) Measured capacitance and calculated depletion width versus bias of a typical 50-μm-diameter $Al_xIn_{1-x}As_ySb_{1-y}$ SACM APD at 300 K. The significant change of capacitance and depletion width at approximately −38 V indicates that electric field has depleted the charge layer and entered into absorption layer.

TABLE I. Parameters used in Monte-Carlo simulation.

Simulation parameters	Electron	Hole
effective mass (m^*/m^0)	0.071	0.35
C_{ii}	8.0×10^{14}	8.0×10^{12}
r	3	3
E_{th}	2	10
Static dielectric constant	15.5	
High frequency dielectric constant	13.7	
Acoustic wave velocity (m/s)	2950	
Acoustic phonon energy (eV)	0.011	
Optical phonon energy (eV)	0.024	
Intervalley phonon energy (eV)	0.013	

gain was achieved with these parameters. The step in the photocurrent near −38 V occurs when the edge of the depletion region reaches the absorbing layer, which is referred as punch-through. The depletion width versus bias was calculated from capacitance measurement at different bias and is shown in Figure 2(b). Figure 3 shows the dark current versus device diameter for bias voltage in the range −30 V to −50 V. The dark current scales with perimeter, which indicates that surface leakage dominates the dark current. To further characterize the dark current, a temperature dependence study from 150 K to 300 K in steps of 25 K was performed with 5 devices. By fitting the dark current (I_{dN}) with temperature (T) exponentially, the activation energy can be determined using the relation[21]

$$I_{dN} \propto T^2 \exp\left(\frac{-E_a}{k_B T}\right), \tag{4}$$

where k_B is the Boltzmann constant and E_a is the activation energy. For this temperature range the activation energy is 0.29 eV ± 0.01 eV, which is approximately half the band-gap of $Al_{0.4}In_{0.6}As_{0.6}Sb_{0.4}$. This indicates that the dark current is primarily generated in the absorption layer through mid-bandgap states.

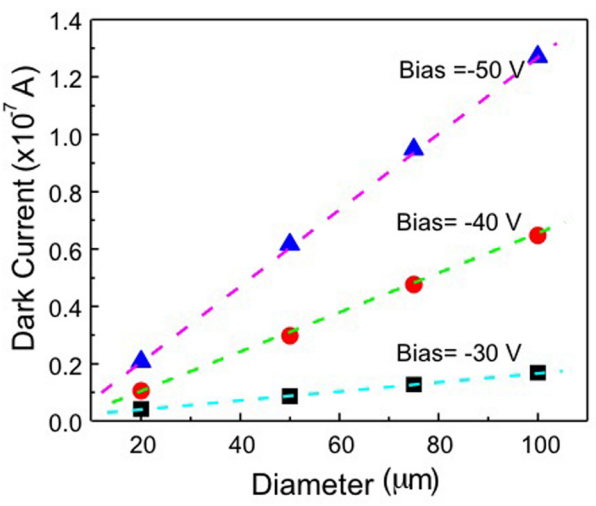

FIG. 3. Dark current size dependence study of $Al_xIn_{1-x}As_ySb_{1-y}$ SACM APDs at 300 K. Results show that dark current increases linearly with diameter of devices at three tested bias, −30 V, −40 V, and −50 V, which indicates that dark current is dominated by surface leakage.

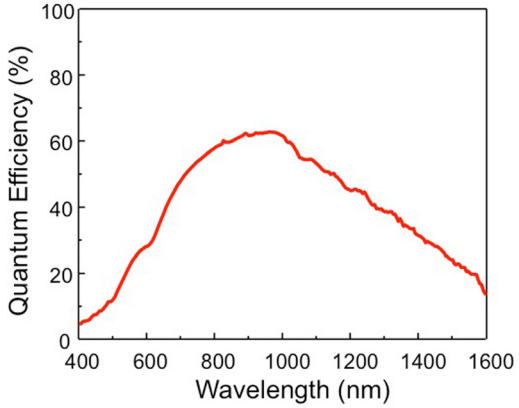

FIG. 4. External quantum efficiency versus wavelength of a 150-μm-diameter $Al_xIn_{1-x}As_ySb_{1-y}$ SACM APD at 300 K.

Owing to the high field in the multiplication layer, there is a small level of impact ionization at punch-through. By fitting the excess noise using the algorithm reported by Liu *et al.*,[22] the gain at punch-through was determined to be 1.7. This fit was confirmed by comparing responsivities with an $Al_{0.4}In_{0.6}As_{0.6}Sb_{0.4}$ control p-i-n photodiode, which has exactly the same 1000 nm absorption layer as the SACM APDs. This is also consistent with measurements of the gain in an $Al_{0.7}In_{0.3}As_{0.3}Sb_{0.7}$ homojunction APD at the same electric field as that of the SACM APD at punchthrough.[16] The normalized external quantum efficiency was measured at −38 V bias using a tungsten-halogen light source, a spectrometer, and a lock-in amplifier. As shown in Figure 4, the optical cutoff wavelength is >1.6 μm. Note that the absorption layer is only 1000 nm thick, there is no anti-reflection coating, and the structure is such that photons make a single pass across the absorber, i.e., there is no "back reflection." Higher quantum efficiency, particularly at longer wavelengths, can be achieved with thicker $Al_{0.4}In_{0.6}As_{0.6}Sb_{0.4}$ absorption layers and by adding an anti-reflection coating to the top surface. Figure 5 shows the excess noise figure F(M),

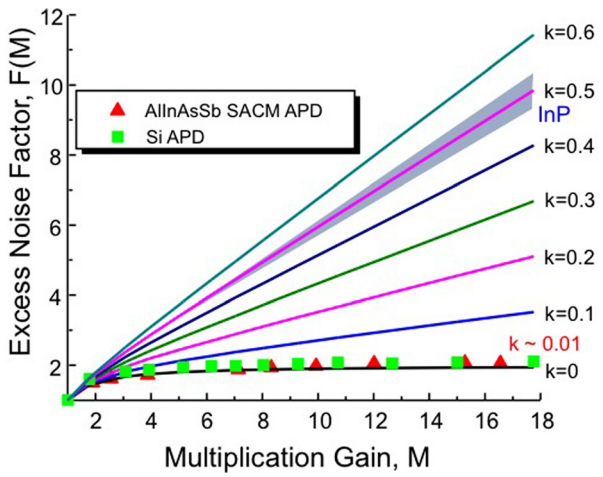

FIG. 5. Measured excess noise factor versus gain for a 50-μm-diameter $Al_xIn_{1-x}As_ySb_{1-y}$ SACM APD (■) and a commercial Si APD (▲). The solid lines are plots of the excess noise factor using the local field model for k values from 0 to 0.6. Both the Si and $Al_xIn_{1-x}As_ySb_{1-y}$ SACM APD are characterized by a k value of ~0.01. The shaded region for k ≥ 0.45 denotes typical values for APDs that employ InP multiplication regions.

as a function of the multiplication gain, for both the $Al_xIn_{1-x}As_ySb_{1-y}$ SACM APD (red triangle) and a commercial Si APD (green square), which were measured by an HP 8970 noise figure meter. The solid lines are plots of the excess noise for k-values from 0 to 0.6 using the local-field model.[4] The measured $Al_xIn_{1-x}As_ySb_{1-y}$ SACM APD excess noise corresponds to an estimated *k*-value of 0.01, which is comparable with or less than that of Si.[23,24]

We report a SACM avalanche photodiodes fabricated from $Al_xIn_{1-x}As_ySb_{1-y}$, grown on GaSb. The excess noise factor of the $Al_xIn_{1-x}As_ySb_{1-y}$ SACM APDs multiplication is characterized by a k value of 0.01, and gain as high as 50 has been achieved. Further, the lattice-matched $Al_{0.4}In_{0.6}As_{0.3}Sb_{0.7}$ absorbing region extends the operating wavelength to the SWIR spectrum. These APDs combine the excellent gain/noise characteristics of Si with the low dark current and high speed of the III-V compound APDs.

This work has been supported by the Army Research Office and DARPA under Contract No. W911NF-10-1-0391.

[1]J. C. Campbell, "Advances in photodetectors," in *Optical Fiber Telecommunications, Part A: Components and Subsystems*, 5th ed., edited by I. Kaminow, T. Li, and A. E. Wilner (Academic Press, 2008), Vol. 5.
[2]J. C. Campbell, J. Lightwave Technol. **34**(2), 278–285 (2016).
[3]T. Fujisawa, S. Kanazawa, K. Takahata, W. Kobayashi, T. Tadokoro, H. Ishii, and F. Kano, Opt. Express **20**, 614–620 (2012).
[4]R. J. McIntyre, IEEE Trans. Electron Devices **ED-13**, 164 (1966).
[5]R. B. Emmons, J. Appl. Phys. **38**, 3705 (1967).
[6]C. Y. Park, K. S. Hyun, S. K. Kang, M. K. Song, T. Y. Yoon, H. M. Kim, H. M. Park, S.-C. Park, Y. H. Lee, C. Lee, and J. B. Yoo, Opt. Quantum Electron. **27**(5), 553–559 (1995).
[7]G. Hasnain, W. G. Bi, S. Song, J. T. Anderson, N. Moll, C.-Y. Su, J. N. Hollenhorst, N. D. Baynes, I. Athroll, S. Amos, and R. M. Ash, IEEE J. Quantum Electron. **34**(12), 2321–2326 (1998).
[8]M. A. Itzler, K. K. Loi, S. McCoy, N. Codd, and N. Komaba, in *LEOS '99, IEEE Lasers and Electro-Optics Society 12th Annual Meeting* (IEEE, San Francisco, USA, 1999), Vol. 2, pp. 748–749.
[9]M. Nada, Y. Muramoto, H. Yokoyama, T. Ishibashi, and H. Matsuzaki, J. Lightwave Technol. **32**, 1543–1548 (2014).
[10]Y. Kang, H.-D. Liu, M. Morse, M. J. Paniccia, M. Zadka, S. Litski, G. Sarid, A. Pauchard, Y.-H. Kuo, H.-W. Chen, W. S. Zaoui, J. E. Bowers, A. Beling, D. C. McIntosh, X. Zheng, and J. C. Campbell, Nat. Photonics **3**, 59 (2009).
[11]Y. Kang, Z. Huang, Y. Saado, J. Campbell, A. Pauchard, J. Bowers, and M. Paniccia, in Optical Fiber Communication Conference/National Fiber Optic Engineers Conference, Paper No. OWZ1, 2011.
[12]N. Duan, T. Liow, A. Lim, L. Ding, and G. Q. Lo, Opt. Express **20**, 11031–11036 (2012).
[13]M. Huang, P. Cai, L. Wang, T. Shi, W. Chen, S. Li, G. Hou, C. Hong, and D. Pan, in Optical Fiber Communication Conference, Paper No. Tu2C.2, 2014.
[14]L. G. Vaughn, L. R. Dawson, E. A. Pease, L. F. Lester, H. Xu, Y. Jiang, and A. L. Gray, Proc. SPIE **5722**, 307–318 (2005).
[15]S. J. Maddox and S. R. Bank, "Broadly tunable AlInAsSb digital alloys grown on GaSb," J. Cryst. Growth Des. (submitted).
[16]M. E. Woodson, M. Ren, S. J. Maddox, Y. Chen, S. R. Bank, and J. C. Campbell, Appl. Phys. Lett. **108**, 081102 (2016).
[17]M. Ren, S. J. Maddox, Y. Chen, M. Woodson, J. C. Campbell, and S. R. Bank, Appl. Phys. Lett. **108**, 081101 (2016).
[18]C. Lenox, P. Yuan, H. Nie, O. Baklenov, C. Hansing, J. C. Campbell, A. L. Holmes, Jr., and B. G. Streetman, Appl. Phys. Lett. **73**, 783 (1998).
[19]F. Ma, S. Wang, X. Li, K. A. Anselm, X. G. Zheng, A. L. Holmes, and J. C. Campbell, "Monte Carlo simulation of low-noise avalanche photodiodes with heterojunctions," J. Appl. Phys. **92**(8), 4791–4795 (2002).
[20]L. V. Keldysh, "Kinetic theory of impact ionization in semiconductors," Sov. Phys. JETP **37**(10), 509–518 (1960).
[21]W. Sun, Z. Lu, X. Zheng, J. C. Campbell, S. J. Maddox, H. P. Nair, and S. R. Bank, IEEE J. Quantum Electron. **49**(2), 154 (2013).
[22]H. Liu, H. Pan, C. Hu, D. McIntosh, Z. Lu, J. C. Campbell, Y. Kang, and M. Morse, J. Appl. Phys. **106**, 064507 (2009).
[23]P. P. Webb, R. J. McIntyre, and J. Conradi, RCA Rev. **35**(2), 234–278 (1974).
[24]V. M. Robbins, T. Wang, K. F. Brennan, K. Hess, and G. E. Stillman, J. Appl. Phys. **58**, 4614–4617 (1985).